

*Supplement of*

## **Liquid-liquid phase separation and viscosity within secondary organic aerosol generated from diesel fuel vapors**

**Mijung Song et al.**

Correspondence to: Allan K. Bertram ([bertram@chem.ubc.ca](mailto:bertram@chem.ubc.ca))

### **Section S1. Simulations of fluid flow for experiments described in Sect. 3.2.1 of the main text**

For these simulations, a quarter-sphere model was used with one of the flat faces of the quarter sphere in contact with the substrate. This model has been described and validated in Renbaum-Wolff et al. (2013). The diameter of the quarter sphere was based on the geometry observed in the experiments. The viscosity in the simulations was adjusted until the amount of movement of the sharp edge of the quarter sphere varied by 0.5  $\mu\text{m}$  in 5 h. As mentioned in the main text, a distance of 0.5  $\mu\text{m}$  corresponds to the minimum amount of movement that could be discerned with in our experiments. Listed in Table S1 are the physical parameters (slip length, surface tension, density, and contact angle) used in the simulations. Viscosities determined in these simulations should be lower limits to the true viscosity for the following reasons: a) the physical parameters using in the simulations were chosen to return conservative lower limits to the viscosities, b) the amount of movement in the experiments was  $\leq 0.5 \mu\text{m}$ , while in the simulations we used 0.5  $\mu\text{m}$ , and c) the particles may have had a higher water content then based on equilibrium with the gas phase due to the relatively short amount of time (1 h) allowed for the particles to condition with the surrounding relative humidity (RH) prior to poking.

### **Section S2. Simulations of fluid flow for experiments described in Sect. 3.2.2 of the main text**

For these simulations, a half-torus geometry was used. This model has been described and validated previously (Renbaum-Wolff et al., 2013; Grayson et al., 2015). The viscosity of the material in the simulations was varied until model flow time,  $\tau_{\text{model, flow}}$ , agreed within 1 % of the experimental flow time,  $\tau_{\text{exp, flow}}$ . Listed in Table S2 are the physical parameters used in

these simulations. The viscosities from these simulations should be lower limits to true viscosities for the following reasons: a) the physical parameters used in the simulations were chosen to return conservative lower limits to the viscosities, b) due to the relatively short amount of time used to condition the particles to the experimental RH, the particles may have had a higher water content than expected based on equilibrium with gas-phase water. If diesel fuel secondary organic aerosol (SOA) is similar to sucrose-water particles in terms of viscosity and diffusion of water, the time used to condition the particles would be sufficient for near equilibrium conditions with gas-phase water (Grayson et al., 2015). However, since the similarity between diesel fuel SOA and sucrose-water particles cannot be guaranteed *a priori*, we assumed that the diesel fuel SOA may not have reached equilibrium with gas-phase water, and the water content of the diesel fuel SOA may have been higher than based on equilibrium with gas-phase water.

### **Section S3. Simulations of fluid flow for experiments described in Sect. 3.2.3**

For these simulations, a two dimensional semicircle with a triangular-shaped crack was used for the initial conditions (Fig. S3a). The bottom of the semicircle (which represented the contact between the particle and the hydrophobic substrate) could deform in the  $x$  direction but not the  $y$  direction. The other interface (which represented the interface between air and the particle) could deform in both  $x$  and  $y$  directions. The diameter of the semicircle used in the simulations was chosen to be consistent with the diameter observed in the experiments. The angle,  $\theta$ , in the crack of the semicircle (Fig. S3a) was set to values ranging from 14 and 20°. Bigger angles were needed for bigger semicircles to ensure the simulations converged. A separate set of simulations showed that changing  $\theta$  from 8° to 34° resulted in a change in the simulated viscosity of only ~10 %.

Parameters used in these simulations are given in Table S3. During the simulations, the material flowed to reduce the surface energy of the system (e.g., Fig. S3). The model recovery time,  $\tau_{model, recovery}$ , was defined as the time when the depth of the crack was 75% of the final height of the initial half circle used in the simulations. The viscosity of the material in the simulations was varied until the depth of the crack was 75 % of the final height when using a simulation time equal to the experimental recovery time,  $\tau_{exp, recovery}$ . Results from these simulations should be upper limits to the true viscosity for the following reasons: a) we used parameters in the simulations that give conservative upper limits to viscosities, b) the model recovery time,  $\tau_{model, recovery}$ ,

1 *recovery* was defined as the time when the depth of the crack was 75% of the final height of the  
2 initial half circle, whereas the  $\tau_{exp, recovery}$ , was defined as the time required for the for the particle  
3 to return to a spherical cap shape, and c) the water content of the particles may have been lower  
4 than expected based on the stabilized gas-phase RH used in the experiments due to the short  
5 amount of time that the particles were exposed to the stabilized gas-phase RH in the  
6 experiments and due to the particles initially being exposed dry conditions (0 % RH) for 1 h.

7 To confirm that these simulations gave upper limits to particle viscosity, we carried out separate  
8 tests using sucrose-water particles. First, a sucrose-water solution (20 wt % sucrose) was  
9 nebulized onto a hydrophobic glass slide to generate sucrose-water particles with diameters of  
10 40 - 100  $\mu\text{m}$ . Experiments were carried out using the same approach as discussed in Sect. 3.2.3,  
11 and simulations were carried out in the same manner as discussed above. Shown in Fig. S4 are  
12 the upper limits to the viscosities of sucrose-water particles at 40 and 50 % RH determined  
13 using this approach. These upper limits are consistent with viscosities of sucrose-water  
14 particles measured by Power et al. (2013) using optical tweezers (Fig. S4).

15

## Tables.

Table S1. Physical parameters used to simulate lower limits of viscosity for poke-and-flow experiments when particles cracked and no flow was observed over 5 h.

Slip length <sup>a</sup> (nm)	Surface tension <sup>b</sup> (mN m <sup>-1</sup> )	Density <sup>c</sup> (g cm <sup>-3</sup> )	Contact angle <sup>d</sup> (°)
5	29	1.4	100

<sup>a</sup> The value of slip length, which is related to the interactions between fluids and solid surfaces, is based on a lower limit to the slip length reported in the literature (Craig et al., 2001; Jin et al., 2004; Joseph and Tabeling, 2005; Joly et al., 2006; Zhu et al., 2012; Li et al., 2014). Viscosity increases in the simulations as the slip length is increased.

<sup>b</sup> The lower limit of the surface tension of diesel fuel-derived SOA were determined as 29 mN m<sup>-1</sup>, the surface tension of diesel fuel at 296 K (Wang et al., 2006). Viscosity increases in the simulations as the surface tension increases.

<sup>c</sup> Density was assumed based on the density of SOA derived from benzene (Ng et al., 2007).

<sup>d</sup> The contact angle of toluene-derived SOA on a hydrophobic substrate is 80-100° based on 3-D fluorescence confocal microscopy (Song et al., 2015). Based on these measurements we assumed an upper limit of 100° for the contact angle for diesel fuel-derived SOA. In the simulations viscosity increases as the contact angle decreases.

Table S2. Physical parameters used to simulate lower limits to the viscosity at 31 and 50 % RH for poke-and-flow experiments.

Slip length <sup>a</sup> (nm)	Surface tension <sup>b</sup> (mN m <sup>-1</sup> )	Density <sup>c</sup> (g cm <sup>-3</sup> )	Contact angle <sup>d</sup> (°)
5	29	1.4	20

<sup>a</sup> The value of slip length, which is the interactions between fluids and solid surfaces, is based on a lower limit to the slip length reported in the literature data (Craig et al., 2001; Jin et al., 2004; Joseph and Tabeling, 2005; Joly et al., 2006; Zhu et al., 2012; Li et al., 2014). Viscosity

increases in the simulations as the slip length increases.

<sup>b</sup> The lower limit of the surface tension of diesel fuel-derived SOA were determined as 29 mN m<sup>-1</sup>, the surface tension of diesel fuel at 296 K (Wang et al., 2006). Viscosity increases in the simulations as the surface tension increases.

<sup>c</sup> Density was assumed based on the density of SOA derived from benzene (Ng et al., 2007).

<sup>d</sup> The contact angle of toluene-derived SOA on a hydrophobic substrate is 80-100° based on 3-D fluorescence confocal microscopy (Song et al., 2015). Based on these measurements we assumed an upper limit of 100° for the contact angle for diesel fuel-derived SOA. In the simulations viscosity increases as the contact angle decreases.

Table S3. Physical parameters used to simulate an upper limit of viscosity for poke-and-flow experiments at 38 and 60 % RH.

Slip length <sup>a</sup> (nm)	Surface tension <sup>b</sup> (mN m <sup>-1</sup> )	Density <sup>c</sup> (g cm <sup>-3</sup> )	Contact angle <sup>d</sup> (°)
10000	75	1.4	80

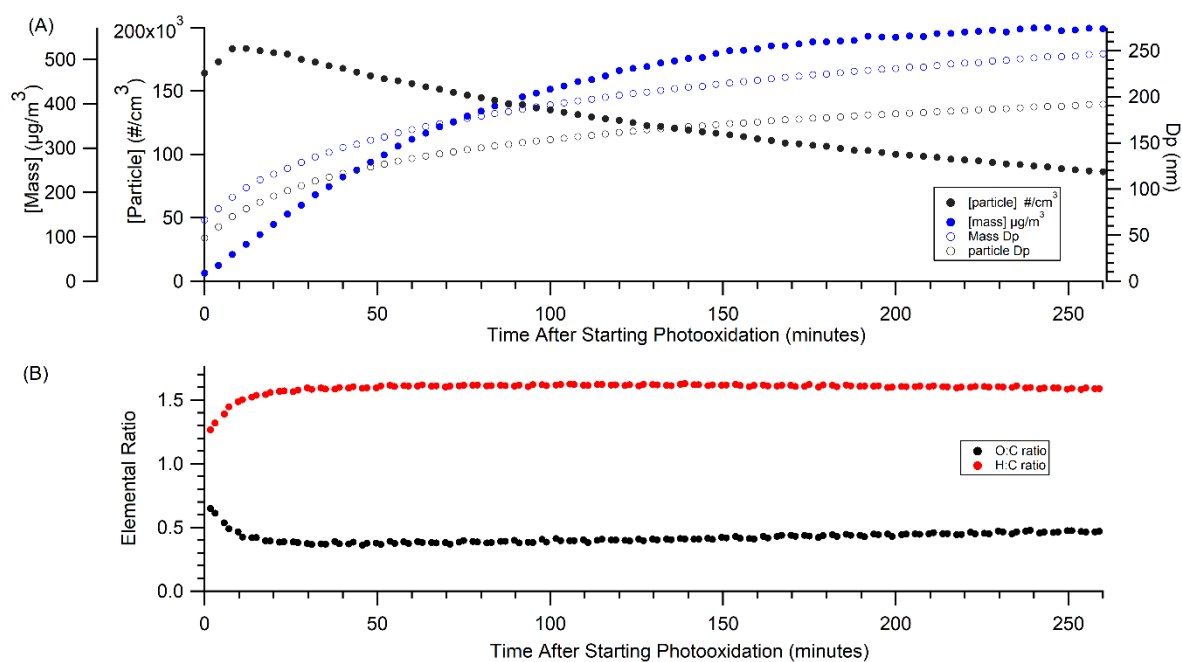
<sup>a</sup> This slip length is an upper limit to the slip length reported in the literature based on previously measured water and organic compound slip lengths on hydrophobic surfaces (Schnell, 1956; Neto et al., 2005; Tretheway and Meinhart, 2002; Choi and Kim, 2006). The viscosities in the simulations decreases as the slip length decreases.

<sup>b</sup> The surface tension was used the surface tension of pure water at 293 K (Engelhart et al., 2008), which should be an upper limit to the surface tension in the experiments. Viscosities decreases in the simulations as the surface tension decreases.

<sup>c</sup> Density was assumed based on the density of SOA derived from benzene (Ng et al., 2007)

<sup>d</sup> The contact angle of toluene-derived SOA on a hydrophobic substrate is 80-100° based on 3-D fluorescence confocal microscopy (Song et al., 2015). Based on these measurements we assumed a lower limit of 80° for the contact angle for diesel fuel-derived SOA. In the simulations viscosity decreases as the contact angle increases.

# 1 **Figures.**



2

3

4 Figure S1. (a) Typical particle number concentration, mass concentration, geometric mean  
5 volume equivalent diameter estimated from mass concentration (Mass Dp), and geometric  
6 mean volume equivalent diameter estimated from particle number concentration (particle Dp)  
7 during diesel fuel photooxidation. Values determined using a scanning mobility particle sizer.  
8 (b) Average elemental ratios measured with a ToF-AMS.

9

RH Decreasing 

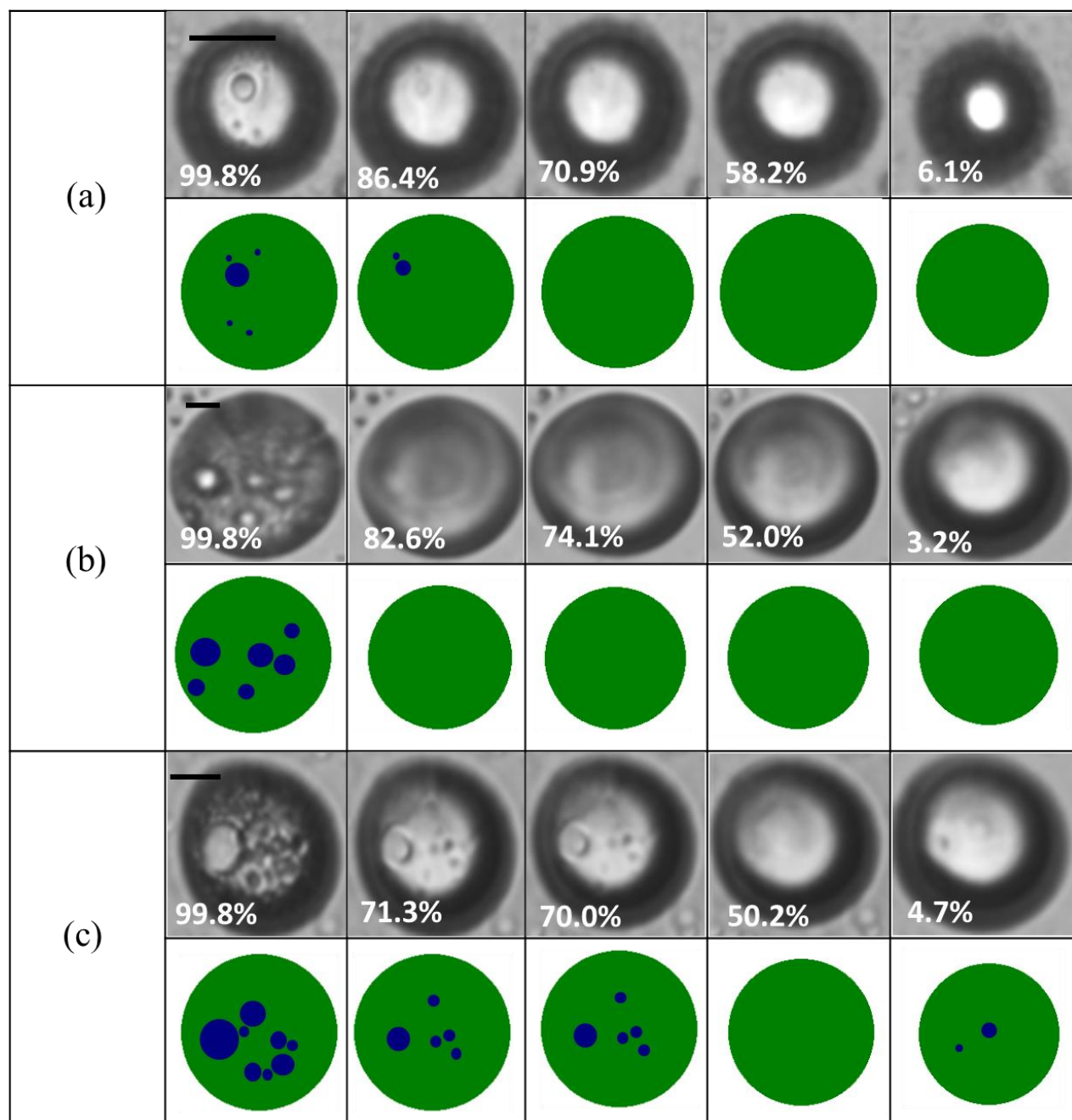


Figure S2. Optical images and illustrations of three different diesel fuel SOA particles for decreasing RH. The illustrations are shown for clarity. Green: Organic-rich phase. Blue: Water-rich phase. The scale bar is 10  $\mu\text{m}$ .

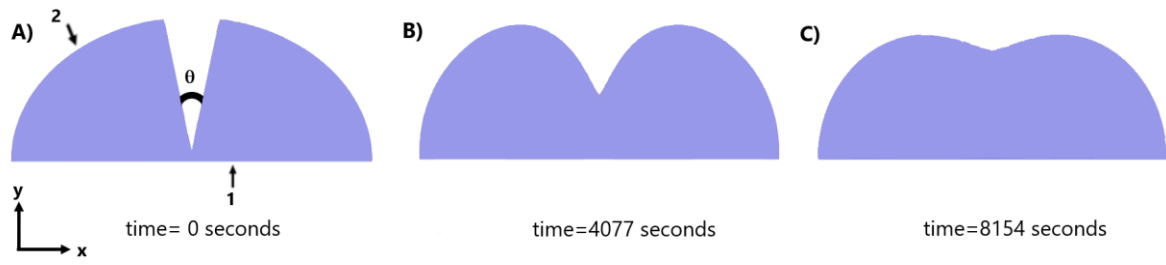


Figure S3. Side view of the geometries from the fluid dynamics simulations at A) the beginning of an experiment, B) after 4077 s, and C) when 75 % of the crack has filled in. In Panel A, interface 1 is the particle-substrate interface and interface 2 is the particle-air interface.



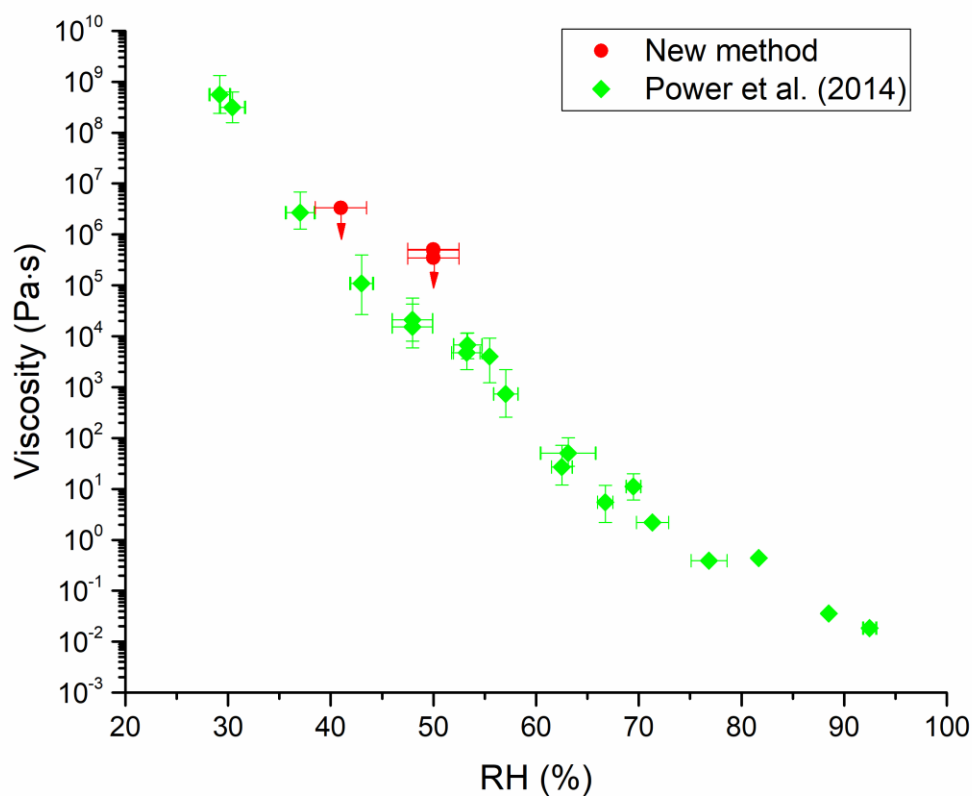


Figure S4. Viscosity as a function of RH for sucrose-water particles. Red dots represent viscosities determined using the new method described in Sections 3.2.3 and S3. Each data point corresponds to a separate experiment. Green dots represent viscosities determined from Power et al. (2013).

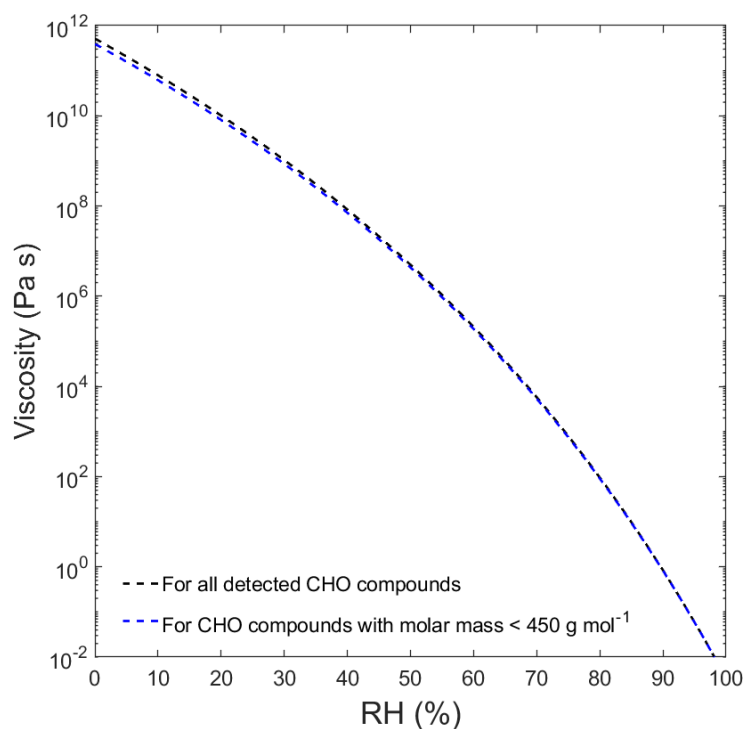


Figure S5. Predicted viscosities of the diesel-derived SOA using Eq. (2) for all the detected CHO compounds (black dashed line, same as that shown in Fig. 3b), and CHO compounds with molar mass  $< 450 \text{ g mol}^{-1}$  (blue dashed line).

## References

- Choi, C. H., and Kim, C. J.: Large slip of aqueous liquid flow over a nanoengineered superhydrophobic surface, *Phys. Rev. Lett.*, 96, Artn 066001 10.1103/PhysRevLett.96.066001, 2006.
- Craig, V. S. J., Neto, C., and Williams, D. R. M.: Shear-dependent boundary slip in an aqueous Newtonian liquid, *Phys. Rev. Lett.*, 87, Artn 054504, Doi 10.1103/Physrevlett.87.054504, 2001.
- Engelhart, G. J., Asa-Awuku, A., Nenes, A., and Pandis, S. N.: CCN activity and droplet growth kinetics of fresh and aged monoterpene secondary organic aerosol, *Atmos. Chem. Phys.*, 8, 3937-3949, 2008.
- Grayson, J. W., Song, M., Sellier, M., and Bertram, A. K.: Validation of the poke-flow technique combined with simulations of fluid flow for determining viscosities in samples with small volumes and high viscosities, *Atmos. Meas. Tech.*, 8, 2463-2472, 2015.

- Jin, S., Huang, P., Park, J., Yoo, J. Y., and Breuer, K. S.: Nearsurface velocimetry using evanescent wave illumination, *Exp. Fluids*, 37, 825–833, doi:10.1007/s00348-004-0870-7, 2004.
- Joly, L., Ybert, C., and Bocquet, L.: Probing the nanohydrodynamics at liquid-solid interfaces using thermal motion, *Phys. Rev. Lett.*, 96, Artn 046101, Doi 10.1103/Physrevlett.96.046101, 2006.
- Joseph, P., and Tabeling, P.: Direct measurement of the apparent slip length, *Phys. Rev. E*, 71, Artn 035303, Doi 10.1103/Physreve.71.035303, 2005.
- Li, L., Mo, J. W., and Li, Z. L.: Flow and slip transition in nanochannels, *Phys. Rev. E*, 90, 033003, doi:10.1103/Physreve.90.033003, 2014.
- Neto, C., Evans, D. R., Bonaccorso, E., Butt, H. J., and Craig, V. S. J.: Boundary slip in Newtonian liquids: a review of experimental studies, *Rep. Prog. Phys.*, 68, 2859-2897, 10.1088/0034-4885/68/12/R05, 2005.
- Ng, N. L., Kroll, J. H., Chan, A. W. H., Chhabra, P. S., Flagan, R. C., and Seinfeld, J. H.: Secondary organic aerosol formation from m-xylene, toluene, and benzene, *Atmos. Chem. Phys.*, 7, 3909-3922, 2007.
- Power, R. M., Simpson, S. H., Reid, J. P., and Hudson, A. J.: The transition from liquid to solid-like behaviour in ultrahigh viscosity aerosol particles, *Chem. Sci.*, 4, 2597-2604, <https://doi.org/10.1039/C3sc50682g>, 2013.
- Renbaum-Wolff, L., Grayson, J. W., Bateman, A. P., Kuwata, M., Sellier, M., Murray, B. J., Shilling, J. E., Martin, S. T., and Bertram, A. K.: Viscosity of alpha-pinene secondary organic material and implications for particle growth and reactivity, *P. Natl. Acad. Sci. USA*, 110, 8014-8019, Doi 10.1073/pnas.1219548110, 2013.
- Schnell, E.: Slippage of Water over Nonwetable Surfaces, *J. Appl. Phys.*, 27, 1149-1152, Doi 10.1063/1.1722220, 1956.
- Song, M., Liu, P. F., Hanna, S. J., Li, Y. J., Martin, S. T., and Bertram, A. K.: Relative humidity-dependent viscosities of isoprene-derived secondary organic material and atmospheric implications for isoprene-dominant forests, *Atmos. Chem. Phys.*, 15, 5145–5159, doi:10.5194/acp-15-5145-2015, 2015.
- Tretheway, D. C., and Meinhart, C. D.: Apparent fluid slip at hydrophobic microchannel walls, *Phys. Fluids*, 14, L9-L12, 10.1063/1.1432696, 2002.
- Wang, F., Wu, J., Liu, Z.: Surface tensions of mixtures of diesel oil or gasoline and dimethoxymethane, dimethyl carbonate, or ethanol, *Energy & Fuels*, 20, 2471-2474,

- 1        10.1021/ef060231c, 2006.
- 2    Zhu, L. W., Neto, C., and Attard, P.: Reliable measurements of interfacial slip by colloid probe
- 3        atomic force microscopy. III. Shear-Rate-Dependent Slip, *Langmuir*, 28, 3465-3473, Doi
- 4        10.1021/La204566h, 2012.